ELSEVIER

Journal of Power Sources 97–98 (2001) 78–82

JOURNAL OF POWER SOURCES

www.elsevier.com/locate/jpowsour

Relation between surface properties, pore structure and first-cycle charge loss of graphite as negative electrode in lithium-ion batteries

Felix Joho[a,*], Beat Rykart[a], Andreas Blome[a], Petr Novák[a], Henri Wilhelm[b], Michael E. Spahr[b]

[a]*Laboratory for Electrochemistry, Paul Scherrer Institute, CH-5232 Villigen PSI, Switzerland*
[b]*TIMCAL GROUP, CH-6743 Bodio, Switzerland*

Received 19 June 2000; accepted 31 December 2000

Abstract

Cycling of graphite in lithium-ion batteries is reversible except for the first-cycle, where some charge is ''lost'' due to irreversible side reactions. The irreversible charge loss of different TIMREX® graphites was found to be a linear function, both of their specific BET surface areas and of the double-layer capacitance of electrodes manufactured from these graphites. Nitrogen-adsorption measurements and differential-porosity calculations indicate that the pore structure of the graphite particles mainly consists of mesopores (2–50 nm). The surface area of these mesopores is part of the electroactive surface area determined by impedance spectroscopy, and contributes to the irreversible capacity of the graphite negative electrode in the first-cycle. © 2001 Elsevier Science B.V. All rights reserved.

Keywords: Lithium intercalation; Graphite; Irreversible capacity; BET surface area; Double-layer capacitance; Graphite pore structure; Lithium-ion battery

1. Introduction

During recent years extensive work has been carried out toward increasing the energy density of lithium-ion batteries. Progress has mainly been made by improving the carbonaceous material of the negative electrode [1] and especially by replacing amorphous coke materials by more highly crystalline graphitic materials. A major problem of the carbonaceous materials is their ''charge loss'' during the first-cycle, which consumes lithium that must be brought into the cell in the form of a relatively heavy lithium metal oxide such as $LiCoO_2$. It is generally accepted that this irreversible charge loss or irreversible capacity seen during the first Li^+ insertion into graphite electrodes is caused by the formation of a solid electrolyte interphase (SEI) on the graphite particles that prevents further electrolyte decomposition at the negative electrode [2,3]. Several research groups began to improve the reversible capacity and reduce the charge loss of graphitic electrodes. But care must be taken when comparing their results, because both the irreversible capacity and reversible specific charge obtained for a graphitic material in a lithium-ion cell depend on experimental conditions such as the cell electrolyte and the design of the electrodes and test cells [4]. In order to learn more about the relationship between graphite material parameters and the performance of these materials as negative electrode materials, we characterised the surface properties of different graphites by gas adsorption measurements and tried to correlate the results with electrochemical charge/discharge and impedance measurements.

2. Experimental

The electrochemical charge/discharge measurements were carried out in the laboratory cells described elsewhere [4]. Electrodes were made, either by doctor-blade coating or by spraying of different TIMREX® graphite materials (TIMCAL GROUP, Bodio, Switzerland), no differences in the electrochemical behaviour of these two types of electrode were seen. PVDF was used as binder material. Electrochemical charge/discharge measurements were performed galvanostatically. We chose relatively low current densities of 10 mA g^{-1} to complete the formation of the solid electrolyte interphase in the first Li^+ insertion cycle. When during the first electrochemical Li^+ insertion a potential of 5 mV versus Li/Li^+ was reached, the charging was continued potentiostatically until the current had dropped

* Corresponding author. Tel.: +41-56-310-21-61; fax: +44-56-310-44-15.
E-mail address: felix.joho@psi.ch (F. Joho).

0378-7753/01/$ – see front matter
PII: S0378-7753(01)00595-X

below 5 mA g^{-1}. Metallic lithium was used as the reference and counterelectrode, 1 M $LiPF_6$ in DMC/EC (LP 30, Merck) was used as the electrolyte solution.

The double-layer capacitance was calculated from the imaginary part of impedance measured at 0.1 Hz. Impedance spectra were recorded at 2.5 V versus Li/Li^+ and a temperature of 298 K with a Zahner IM6 impedance spectrometer at an ac signal amplitude of 10 mV. The cell components were arranged as in button cells, and fitted with a lithium reference electrode as published elsewhere [5]. The compression spring was isolated from the electronic circuit with PTFE caps, and instead of the spring, a copper wire was used to make the electronic contact.

Nitrogen adsorption measurements were performed, either with a Ströhlein Areameter 2 apparatus for the usual BET surface area determination or a Micromeritics ASAP 2010 apparatus for determination of the pore size distribution. Owing to differences in the experimental conditions, the surface areas measured with the Ströhlein apparatus are systematically higher than those measured with the Micromeritics ASAP 2010 apparatus. Samples were evacuated until a static vacuum of less than 7 μm Hg was reached. The Brunauer–Emmett–Teller (BET) transform was calculated with ASAP software. We also used DFT+ software, an enhanced data reduction application provided by Micromeritics. In the isotherm deconvolution according to density functional theory (DFT), either the porosity or the surface energy of the solid is taken into account. These calculations have been successfully applied to isotherms obtained on graphitised materials [6,7].

3. Results and discussion

The irreversible capacity seen during the first reduction cycle affects the available capacity of a lithium-ion cell [8]. On the other hand, an ideal solid electrolyte interphase that is formed as a surface film is essential for the functioning of the graphite negative electrode. This means that SEI formation must be as effective as possible so as to keep the charge losses as small as possible. It is almost universally accepted in the literature [9,10] that the irreversible charge loss occurring during the first reduction cycle depends on the electrode surface area and on the specific BET surface area of the graphite material used in the negative electrode, because the SEI covers all the surface area exposed to the electrolyte solution.

Fig. 1 shows the irreversible capacities of the first charge/discharge cycle plotted as a function of the BET surface areas determined for synthetic TIMREX® graphites of the KS, SFG, T, E-SLX and SLM type as well as for the natural graphite TIMREX® E-NP 15. It can be seen that this function is linear. A linear regression fit of the experimental data resulted in a correlation factor, R^2 of 95%. It must be pointed out, however, that the experimental conditions are very important for consistent and reproducible results. We

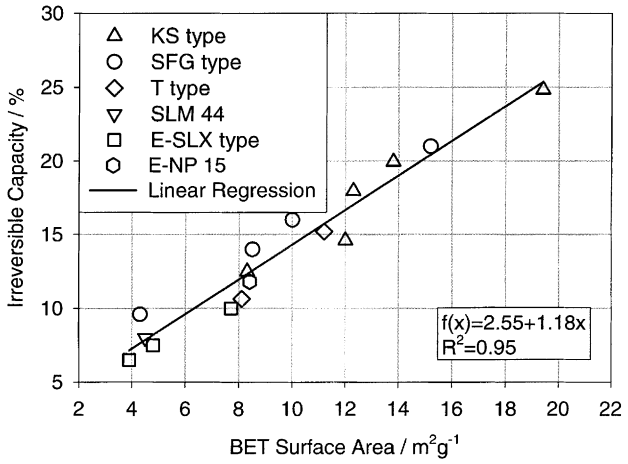

Fig. 1. Irreversible capacities of the first electrochemical Li^+ intercalation into different synthetic and natural TIMREX® graphites as a function of the specific BET surface areas measured at 10 mA g^{-1} in a 1 M $LiPF_6$, EC:DMC (1:1) electrolyte.

chose a small specific current (about C/36) and room temperature for galvanostatic charging of the cell in the first-cycle in order to complete formation of the SEI layer and maximise the irreversible capacity in the first-cycle of the electrode.

The first-cycle of an electrode containing TIMREX® E-SLX 50 as the active material is presented as an example in Fig. 2. It shows a galvanostatic charge/discharge curve typical for highly crystalline graphite electrode materials, with reversible Li^+ intercalation/deintercalation occurring at potentials below 0.2 V versus Li/Li^+. The SEI formation takes place at potentials between 0.8 and 0.2 V versus Li/Li^+ in the Li^+ insertion (charging) half cycle. The specific BET surface area of this sample was 3.9 $m^2\ g^{-1}$. The first charging of the electrode consumed 385 Ah kg^{-1}, while the reversible capacity was 360 Ah kg^{-1}. The charge loss or

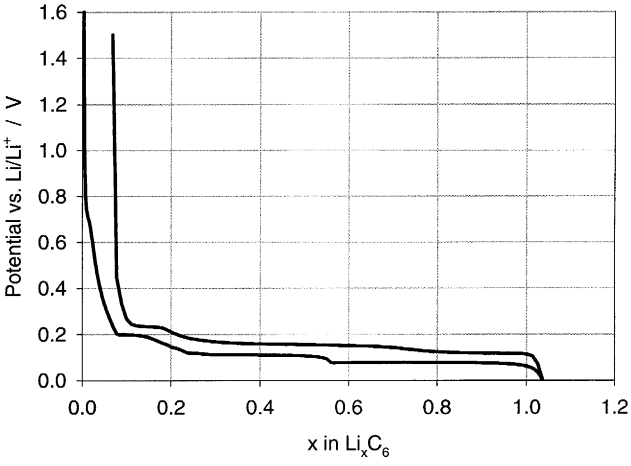

Fig. 2. First galvanostatic charge/discharge cycle of a TIMREX® E-SLX 50 negative electrode at 10 mA g^{-1} graphite in a 1 M $LiPF_6$, EC:DMC (1:1) electrolyte.

irreversible capacity C_{irrev} of this sample as calculated by the formula

$$C_{irrev} = \frac{C_{int} - C_{rev}}{C_{int}}$$

was 6.5%; here C_{irrev} is the irreversible capacity in %, C_{int} the specific charge recorded in the first Li^+ intercalation, and C_{rev} the reversible specific charge recorded in the corresponding Li^+ deintecalation.

Electrodes containing the different TIMREX® graphites all exhibited reversible capacities of more than 360 Ah kg^{-1} at a specific current of 10 mA g^{-1} (both figures being referred to the mass of graphite in the negative electrode). The data obtained for the irreversible capacity in the galvanostatic charge/discharge experiments as well as for the double-layer capacitance obtained from impedance measurements are summarised in Table 1.

A linear function is also obtained when the charge losses or irreversible capacities of graphite electrodes containing the same TIMREX® graphites are plotted against their double-layer capacitance as determined by impedance spectroscopy (Fig. 3). Here the correlation factor was 96%. For a reliability test of our results, the double-layer capacitance found in all 38 measurements were divided by the corresponding specific BET surface areas. From this calculation we obtained an average double-layer capacitance of ca. 4 μF cm^{-2}.

There are some differences between the two plots: irreversible charge loss versus specific BET surface areas (Fig. 1) and irreversible charge loss versus double-layer capacitance (C_{dl}) (Fig. 3), but the linear regression fit is equivalent. The instances of departure of the data from the straight-line fit might be attributed to a material parameter other than the BET surface areas. However, it is not certain whether these deviations are significant. Moreover, in some cases the results reported in the present paper are inconsistent

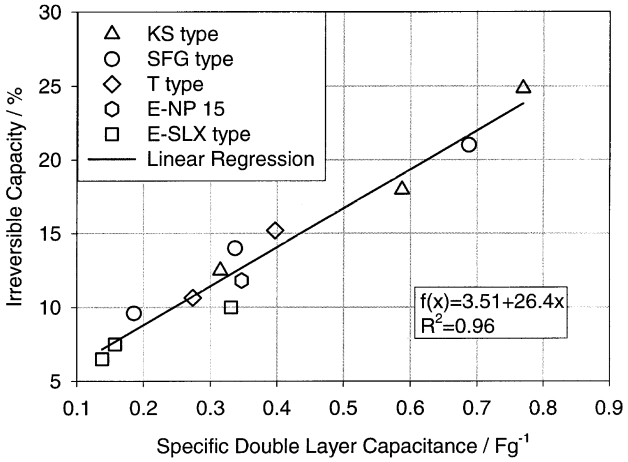

Fig. 3. Irreversible capacities of the first electrochemical reduction of different synthetic and natural TIMREX® graphite electrodes as a function of their double-layer capacitance calculated from impedance spectroscopic measurements at 2.5 V vs. Li/Li^+.

with results obtained in our laboratory some years ago [11]. Differences in electrode manufacturing and in the experimental set-up may be responsible for these differences. For the present studies we had optimised the structure of the negative electrode so as to obtain the maximum reversible specific capacity. By improved electrode manufacturing we could ensure that all particles of the electroactive material in the electrodes fully participated in the electrochemical reaction. Also, the drying conditions for the electrodes before cell assembly were improved, since water contamination of the electrolyte has a significant influence on the irreversible charge loss seen during the first-cycle [4].

In this context, it is remarkable that TIMREX® graphites of the SFG type have relatively high irreversible capacities, while graphites of the E-SLX type have relatively low irreversible capacities.

Table 1
Surface properties and results of electrochemical charge/discharge measurements and impedance spectroscopic studies of different synthetic and natural TIMREX® graphites

Product	Specific BET surface area ($m^2 g^{-1}$)	Charge loss (%)	Specific capacitance, C_{dl} (F g^{-1})	d_{50} (μm)
KS 6	19.4	24.8	0.769	3.6
KS 10	13.8	20.0		5.6
KS 15	12.3	18.0	0.587	7.5
KS 25	12.0	14.6		8.2
KS 44	8.3	12.5	0.315	16.2
SFG 6	15.2	21.0	0.688	3.4
SFG 10	10.0	16.0		5.8
SFG 15	8.5	14.0	0.337	7.5
SFG 44	4.3	9.6	0.186	23.6
T 15	11.2	15.2	0.397	8.6
T 44	8.1	10.7	0.273	20.2
SLM 44	4.5	8.0		24.0
E-SLX 20	7.7	10.7	0.331	10.2
E-SLX 30	4.8	7.5	0.157	18.5
E-SLX 50	3.9	6.5	0.138	28.0
E-NP 15	8.4	11.8	0.347	9.1

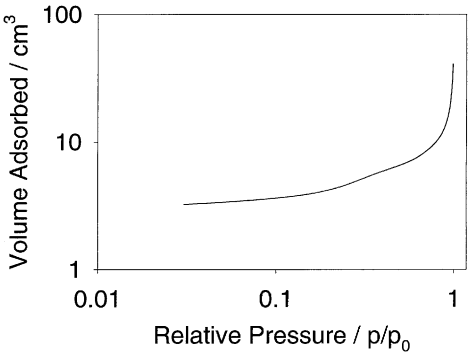

Fig. 4. Nitrogen gas adsorption isotherm of TIMREX® SFG 15. The shape of this isotherm is similar to that found for the other TIMREX® samples, and typical for materials with a pore structure containing mainly mesopores.

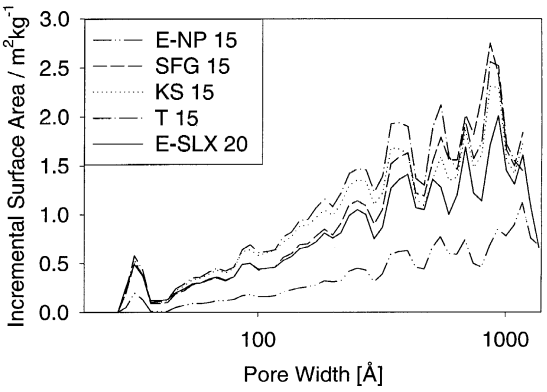

Fig. 5. Pore structures of different synthetic and natural TIMREX® graphites: incremental surface areas as a function of the pore width calculated from DFT porosity calculations based on data taken from nitrogen gas adsorption measurements.

For a better understanding of the mechanism of SEI formation at the graphite particle surface, differential-porosity measurements were performed using different TIMREX® graphite types having approximately the same particle-size distributions. Fig. 4 shows a typical isotherm obtained in the gas absorption measurements of these graphites. The shape of this isotherm is typical for materials with a high content of mesopores (typical pore widths of 2–50 nm). Two DFT models (porosity and surface energy) have been applied to the isotherms. The pore-size distributions obtained with the porosity model indicate that the graphite materials mainly consist of mesopores. The pore structures of the synthetic and natural graphite samples examined are similar. Interestingly, however, the DFT porosity calculations indicate that mesoporosity is more pronounced in the synthetic TIMREX® graphite samples (E-SLX, SFG, KS and T) than in natural graphite TIMREX® E-NP 15 (Fig. 5). This result was confirmed, when comparing surface area values calculated with DFT porosity model and with BET transforms (Table 2). The largest deviation is seen for the natural graphite sample, indicating that here the porosity model is definitively inappropriate. For the natural graphite TIMREX® E-NP 15, the surface energy model appears to be more appropriate, since it leads to a satisfactory agreement between the measured BET value and the surface area calculated by means of DFT surface energy theory. These results indicate that the mesopores of TIMREX® E-NP 15 make a smaller contribution to the BET surface area and, thus, to the irreversible capacity of the first reduction cycle than those of the synthetic graphites examined. However, the total BET surface area measured for the natural graphite TIMREX® E-NP 15 is in the same range as the BET surface areas obtained for the synthetic graphites TIMREX® E-SLX 20 and SFG 15.

The irreversible capacity found for natural graphite nicely adheres to the linear relations of Figs. 1 and 3 linking the charge loss to BET surface areas and double-layer capacitance. This indicates that the geometrical surface area of the natural graphite particle excluding the mesopores contributes more to the BET surface area and to the irreversible capacity of the first electrochemical reduction than that of the synthetic graphites. Obviously, natural graphite differs from the synthetic graphites examined, not only in its mesoporosity, but also in its surface morphology, i.e. roughness of the particle surface and defects on the particle surface. The synthetic graphite samples exhibit more highly developed mesoporosity, while the natural graphite sample has a rougher surface, so that similar values are recorded for their BET surface areas and for the irreversible capacities in the first reduction of the corresponding graphite negative electrodes.

Table 2
Comparison of the specific BET surface areas with the surface areas obtained from the DFT porosity and surface energy model calculations[a]

	BET surface area ($m^2\ g^{-1}$)	Surface area (porosity model) ($m^2\ g^{-1}$)	Surface area (surface energy model) ($m^2\ g^{-1}$)
E-SLX 20	6.8	7.8	14.1
SFG 15	8.1	8.7	16.0
T 15	10.7	10.7	18.8
KS 15	11.5	10.4	18.0
E-NP 15	7.7	4.0	7.7

[a] The listed BET surface areas were obtained from nitrogen adsorption measurements, and differ slightly from the BET surface areas in Fig. 1 measured by single point nitrogen adsorption.

4. Conclusion

Results of nitrogen gas absorption measurements performed with different synthetic and natural TIMREX® graphites indicated that the porosity of highly crystalline graphites mainly consists of mesopores. The irreversible capacities of the first Li^+ intercalation in graphite negative electrodes linearly depend on both the specific BET surface areas of the graphite materials and the double-layer capacitance of the corresponding graphite electrodes. Since the specific BET surface areas and double-layer capacitance also exhibit a linear relationship, we conclude that the surface area of the graphite mesopores contributes to the electroactive surface, i.e. almost all graphite mesopores determined by gas adsorption are wetted by the liquid electrolyte solution used in lithium-ion batteries.

The results of DFT calculations based on nitrogen gas adsorption measurements indicate that the pore structures and surface morphologies of the synthetic graphites investigated are significantly different from those of the natural graphite sample. The contribution of mesoporosity to the irreversible capacity of a graphite electrode is larger in the case of synthetic graphites. However, the surface morphology of the natural graphite differs from that of the synthetic graphites. The surface of the natural graphite particles is rougher, thus, makes a larger contribution to the BET surface area and to the irreversible capacity of the electrochemical reduction cycle than that of the synthetic graphite materials.

References

[1] A. Yoshino, Abstract ISIC 10 (1999) 31A5, Okazaki, Japan.
[2] E. Peled, in: J.-P. Gabano (Ed.), Lithium Batteries, Academic Press, London, 1983, p. 43.
[3] J.R. Dahn, A.K. Sleigh, H. Shi, B.M. Way, W.J. Weydanz, J.N. Reimers, Q. Zhong, U. von Sacken, in: G. Pistoia (Ed.), Lithium Batteries, New Materials, Developments, and Perspectives, Elsevier, Amsterdam, 1994, p. 1.
[4] F. Joho, B. Rykart, R. Imhof, P. Novák, M.E. Spahr, A. Monnier, J. Power Sources 81/82 (1999) 243.
[5] P. Novák, W. Scheifele, F. Joho, O. Haas, J. Electrochem. Soc. 142 (1995) 2544.
[6] J.P. Olivier, J. Porous Mater. 2 (1995) 9.
[7] J.P. Olivier, Carbon 36 (1998) 1469.
[8] M. Broussely, P. Biensan, B. Simon, Electrochim. Acta 45 (1999) 3.
[9] R. Fong, U. von Sacken, J.R. Dahn, J. Electrochem. Soc. 137 (1990) 2009.
[10] B. Simon, S. Flandrois, A. Février-Bouvier, P. Biensan, Mol. Cryst. Liq. Cryst. 310 (1998) 333.
[11] M. Winter, P. Novák, A. Monnier, J. Electrochem. Soc. 145 (1998) 428.